Science Advances
AAAS

advances.sciencemag.org/cgi/content/full/6/38/eabc4886/DC1

Supplementary Materials for

Chaos-assisted tunneling resonances in a synthetic Floquet superlattice

M. Arnal, G. Chatelain, M. Martinez, N. Dupont, O. Giraud, D. Ullmo, B. Georgeot, G. Lemarié, J. Billy, D. Guéry-Odelin*

*Corresponding author. Email: dgo@irsamc.ups-tlse.fr

Published 18 September 2020, *Sci. Adv.* **6**, eabc4886 (2020)
DOI: 10.1126/sciadv.abc4886

This PDF file includes:

Supplementary Materials

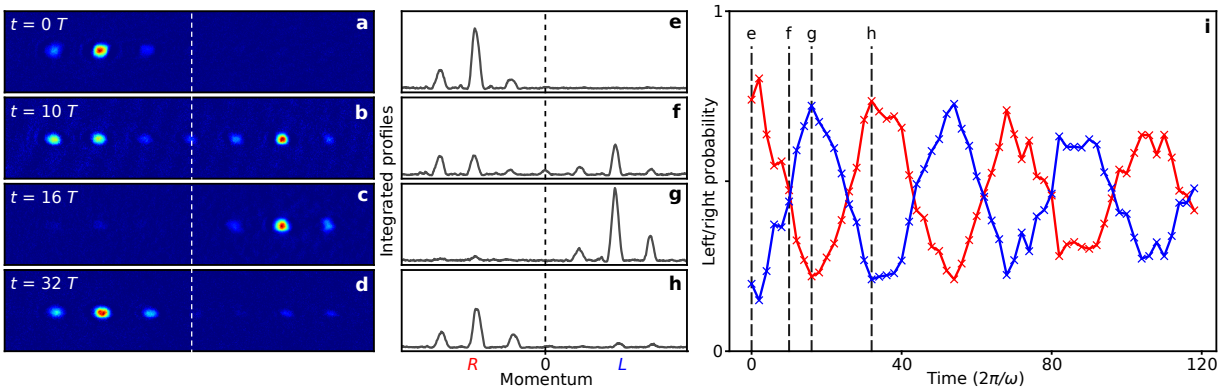

Fig. S1. Determination of the populations in the left and right islands. a-d, Experimental absorption images taken after a 25 ms time-of-flight for different numbers of modulation period. **e-h**, Solid lines: profiles of the experimental images integrated along the vertical axis, giving access to the momentum distribution along the lattice axis (the dashed line separates the positive and negative momentum components). **i**, Time-evolution of the population of the right (red color) (resp. left (blue color)) regular island obtained from the integration of the momentum profiles (e.g. **e-h**) over negative (resp. positive) momenta.

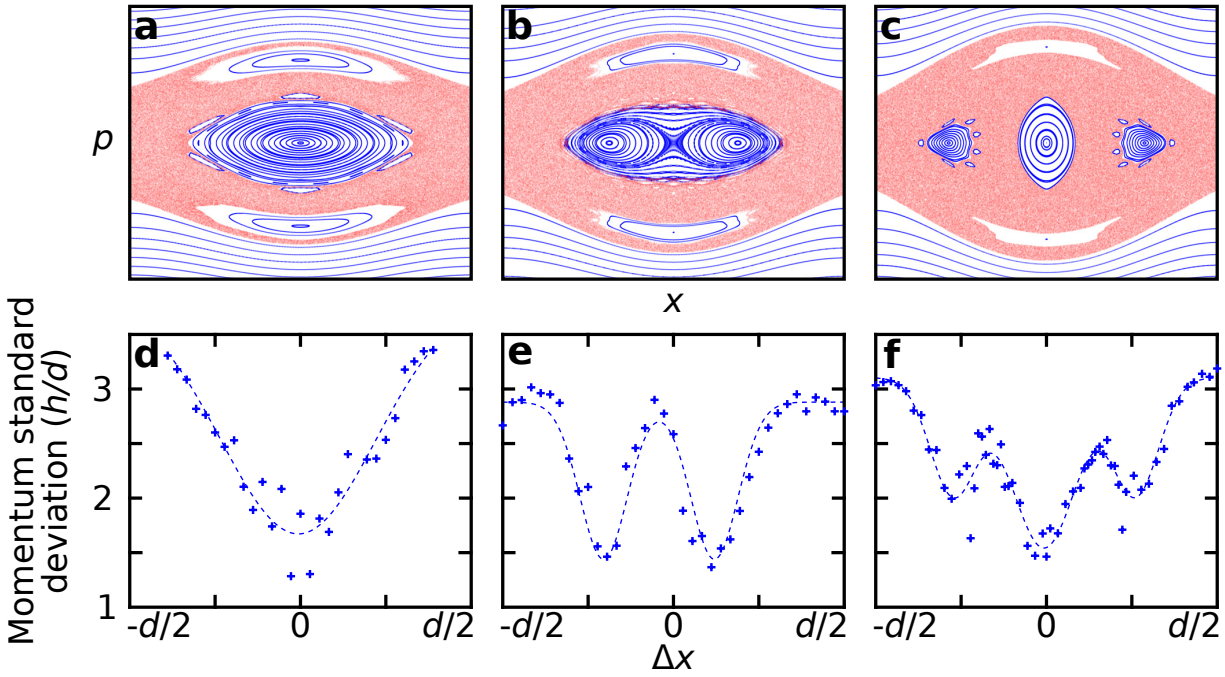

Fig. S2. Determination of regular island(s) position(s). Phase space generated by the parameters $\varepsilon = 0.268$ and **a** $\gamma = 0.188$, **b** $\gamma = 0.265$, **c** $\gamma = 0.348$, showing the splitting of the central regular island into two and three islands. **d-f**, Experimental results associated to each phase space: the standard deviation of the atomic momentum distribution is plotted as a function of the in-trap initial position Δx of the atomic wave packet. Dotted lines: multi-Gaussian fits.

1. Bifurcation and rotation in phase space

The bifurcation - To introduce the main features of the bifurcation, we linearize the classical equation of motion close to x=0 and introduce explicitly the period of modulation T. In this way, we get at third order of expansion the Mathieu-Duffing equation:

$$\frac{dp}{dt} + \gamma\left(1 + \varepsilon\cos\left(2\pi\frac{t}{T}\right)\right)\left(x - \frac{x^3}{6}\right) = 0 \qquad \text{(S1)}$$

The standard linear Mathieu equation displays instabilities (unbounded solutions) for a discrete set of ratios between the forcing and the natural frequencies (proportional to $\sqrt{\gamma}$). The non-linearities of Eq. (S1) shifts those resonances and can even restore their stability. This latter effect is responsible for the bifurcation.

According to the analytical approach developed in Refs. *(40,69)*, the bifurcations occur at two critical values $\gamma_c = (4 \pm 2\varepsilon)^{-1}$. For a fixed amplitude of modulation ε, the first bifurcation when the lattice depth γ is increased amounts to breaking the central stable island into two off-centered symmetric stable islands whose phase space coordinates are given by

$$\begin{pmatrix} x^* \\ p^* \end{pmatrix} = \pm\sqrt{8\left(1 + \frac{\varepsilon}{2} - \frac{1}{4\gamma}\right)}\begin{pmatrix} \cos(\pi t/T) \\ \sin(\pi t/T)/2 \end{pmatrix} \qquad \text{(S2)}$$

For our parameter ($\varepsilon = 0.268$), this bifurcation occurs at $\gamma = 0.22$. In the range $0.22 < \gamma < 0.29$, the (x,p)=(0,0) orbit becomes unstable. For $\gamma > 0.29$, the stability of this orbit is restored (see Fig. **2** of the main text).

Rotation in phase space and $2T$ *formalism* - Equation (S2) actually describes the forced motion of a pair of stable points in the (x,p) plane. They rotate with a $2T$ period on an ellipse centered on (x,p)=(0,0) (see Fig. **S3**). This is the reason why (i) we probe the system stroboscopically every $2T$ and (ii) we wait for an extra T/2 period to transfer the information from the x-axis to the p-axis.

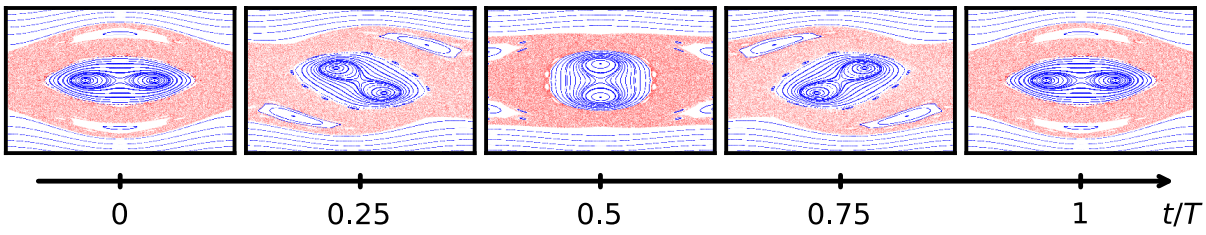

Fig. S3. Rotation of the stable orbits in phase space. Stroboscopic phase spaces are plotted for different values of the modulation time showing the rotation of the two symmetric islands. Parameters: $\varepsilon = 0.15$, $\gamma = 0.25$.

2. Additional experimental CAT resonances

CAT resonances are a very generic feature of mixed systems. We report hereafter two other observations performed with different parameters showing three additional resonances (see Figs. **S4** and **S5**). The experimental data are in very good agreement with the numerical simulations.

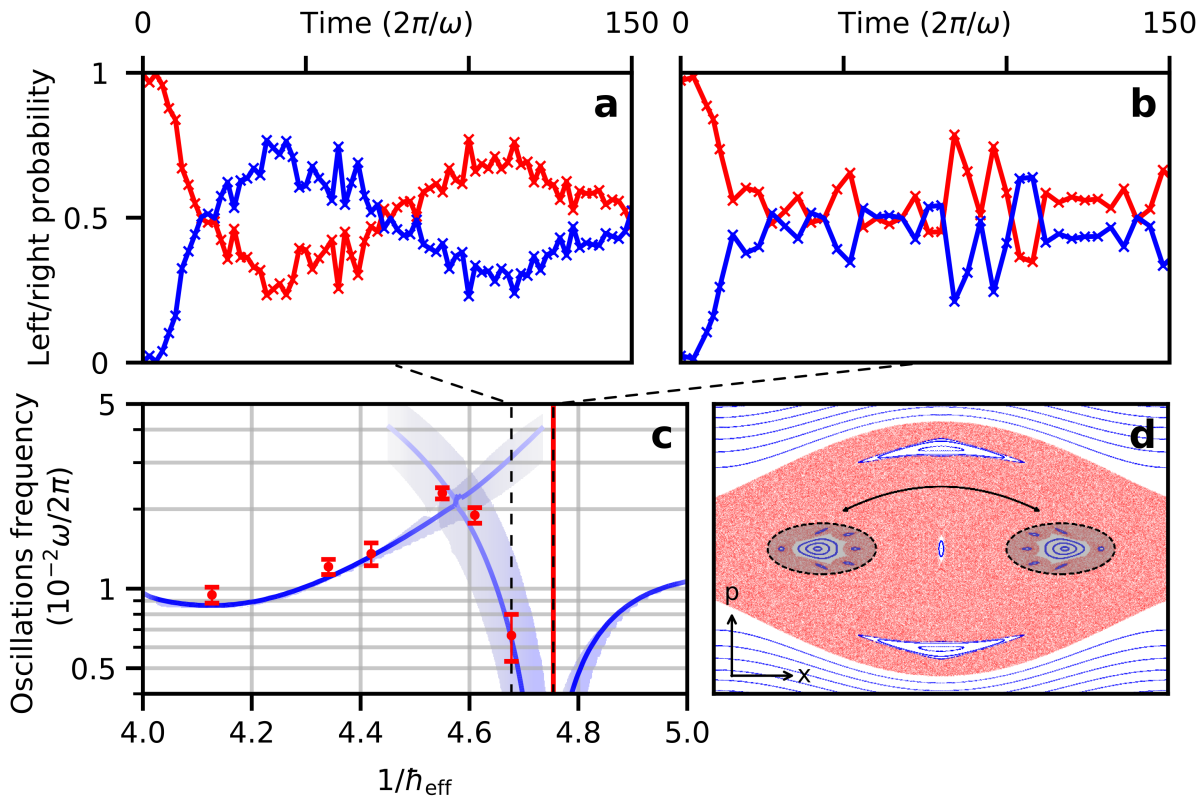

Fig. S4. Second experimental CAT resonance. **a-b**, Examples of experimental tunneling oscillations. **c**, Experimentally measured tunneling frequencies (red dots) as a function of the inverse of the effective Planck constant compared to the theoretical/numerical predictions corresponding to $\gamma = 0.315 \pm 0.005$ and $\varepsilon = 0.39$. The vertical red line indicates a dataset right at resonance for which we couldn't extract a frequency. The blue shaded area corresponds to the experimental uncertainty on γ. The corresponding classical phase space is plotted in **d**.

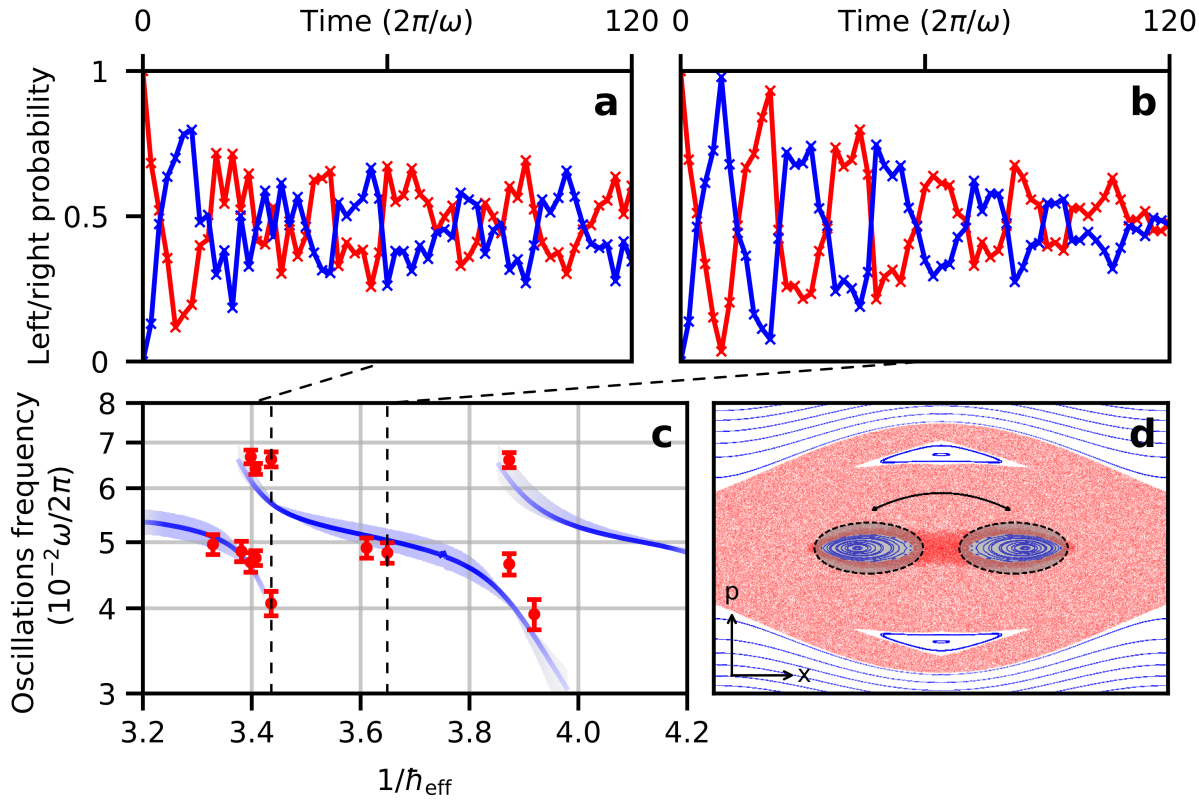

Fig. S5. Third and fourth experimental CAT resonances. **a-b**, Examples of experimental tunneling oscillations. **c**, Experimentally measured tunneling frequencies (red dots) as a function of the inverse of the effective Planck constant compared to the theoretical/numerical predictions corresponding to $\gamma = 0.229 \pm 0.001$ and $\varepsilon = 0.60$. The blue shaded area corresponds to the experimental uncertainty on γ. The corresponding classical phase space is plotted in **d**.

3. Spectrum and eigenstates analysis of the experimental CAT resonances

The theoretical description of chaos-assisted tunneling resonances involves an avoided crossing scenario between regular and chaotic states. This description rests on the semi-classical approximation (effective Planck constant small enough compared to the size of the classical structures of the phase space) that guarantees to be able to label chaotic and regular states. For the three experimental configurations we probed, the quasi-energy spectra show avoided crossings associated with the observed resonances (see Figs. **S6a**, **S7a**, **S8a)** and the states involved can be labelled in two classes: regular (see Figs. **S6b-c**, **S7 b-c**, **S8 b-c**) and chaotic (see Figs. **S6d-e** , **S7d-e** , **S8d-e**).

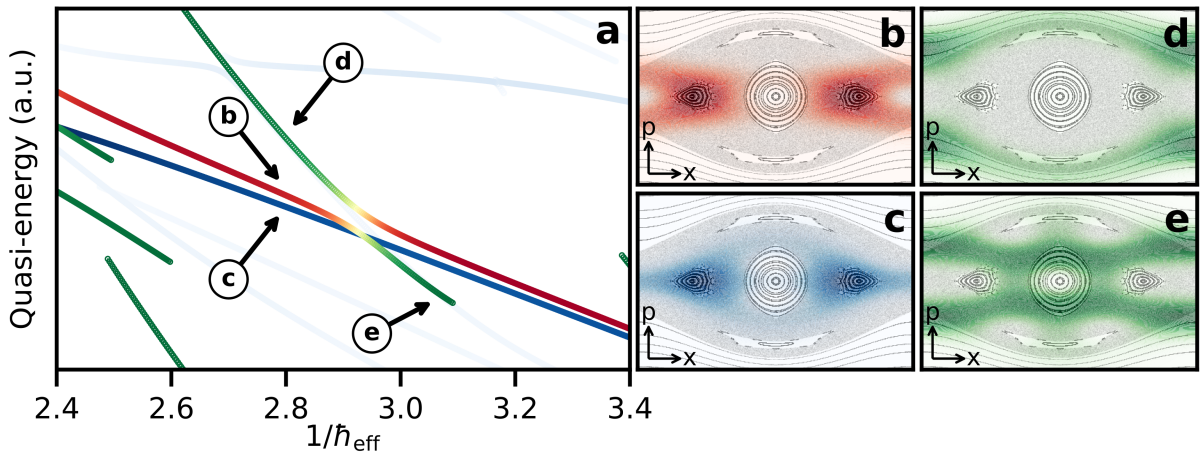

Fig. S6. Eigenstates analysis of the first experimental CAT resonance (see Fig. **4** of main text). **a**, quasi-energy spectrum of the quantum states involved in the CAT resonance. To identify the relevant eigenstates, we compute their overlap with a Gaussian state placed at the center of one of the lateral islands. In blue: regular eigenstate having a given parity. In red: regular eigenstate with the opposite parity. In green: chaotic states. Red (regular state) to green (chaotic state) curves reveal the mixing between regular and chaotic states having the same parity (avoided crossing). **b, c, d, e** Husimi distribution of the relevant eigenstates superimposed to the classical phase space.

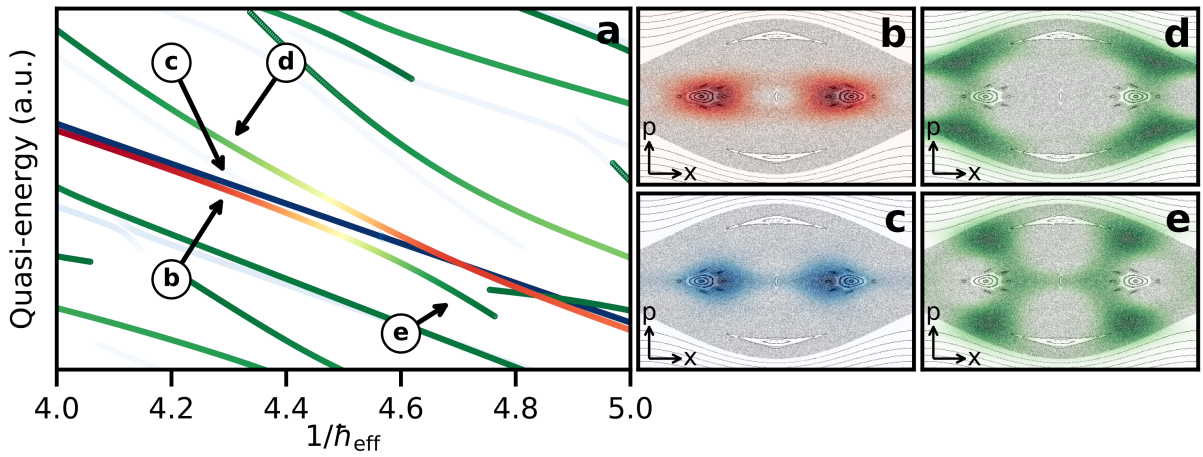

Fig. S7. Eigenstates analysis of second experimental CAT resonance (see Fig. **S4**). Same convention as Fig. **S6**.

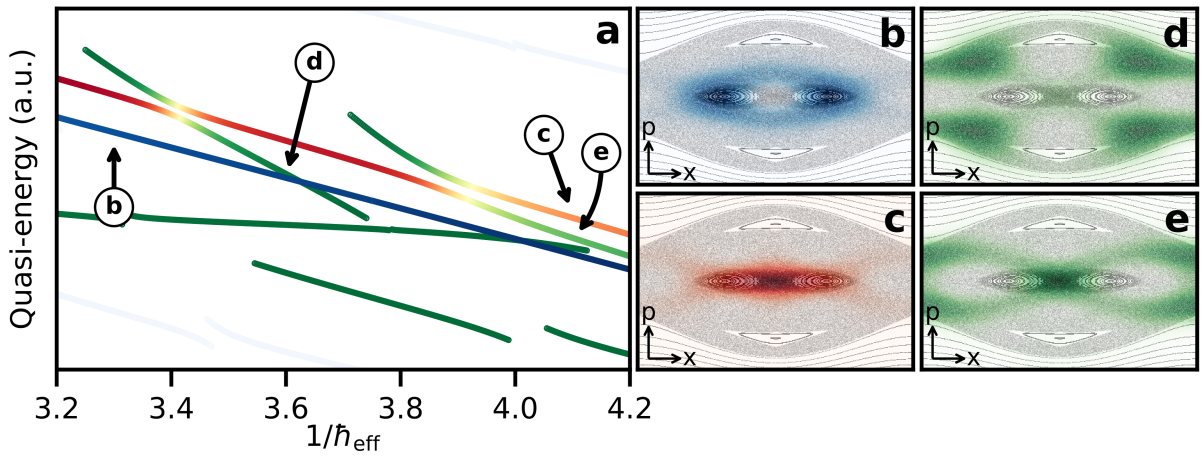

Fig. S8. Eigenstates analysis of the third and fourth experimental CAT resonances (see Fig. **S5**). Same convention as Fig. **S6**.

4. Oscillation damping

As stated in the main article, the number of atoms in the condensate drastically affects the damping of the chaos-assisted tunneling oscillations (see Fig. **S9**). We attribute this effect to the dephasing of BECs in each lattice site due to interatomic interactions. As the strength of the interaction depends on the density, reducing the number of atoms decreases the damping rate.

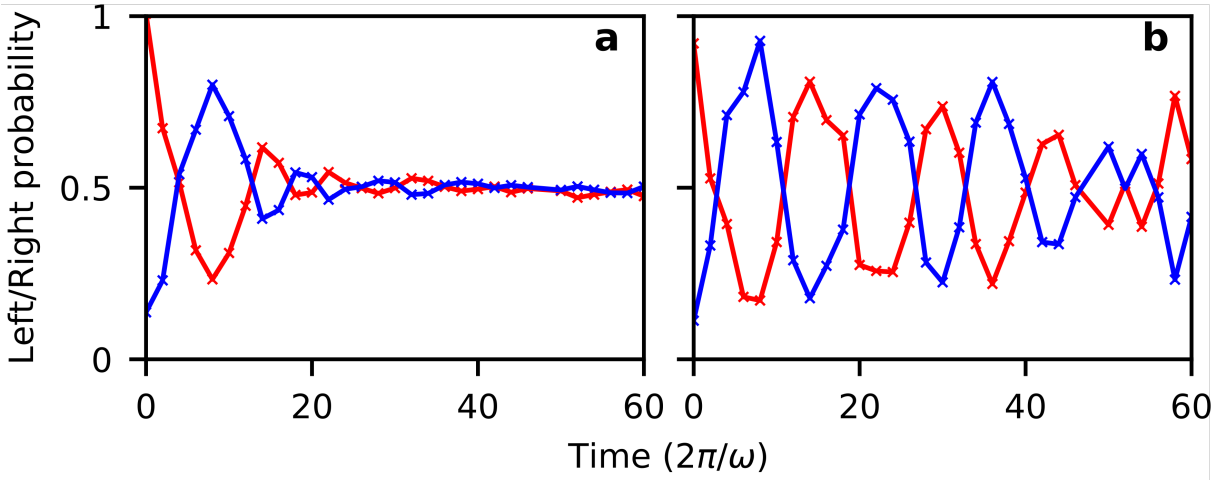

Fig. S9. Damping of oscillations with the number of atoms. Comparison of the chaos-assisted tunneling oscillations for two different atom numbers: **a** $N = 1.2 \pm 0.2 \times 10^5$ and **b** $N = 4 \pm 0.2 \times 10^4$. The phase space parameters are $\gamma = 0.225 \pm 0.005$ and $\varepsilon = 0.59 \pm 0.01$.

More specifically, with 10^5 atoms spread over 30 lattice cells, it corresponds to about 3000 atoms per site. In a lattice well, the frequencies are equal to 40 Hz along the transverse axes and on the order of 30 kHz along the lattice direction. With such figures, the Thomas-Fermi radius is close to 20 nm along the lattice direction (well below the lattice spacing equal to 532 nm). The atomic density in a cell of the lattice is typically on the order of 4×10^{14} atoms per cm^3 which set the dimensionless parameter $na^3 \sim 5.2 \times 10^{-5} \ll 1$, where n is the atomic density and a = 5.35 nm is the rubidium-87 scattering length associated to the internal state F=1,m_F=-1. The BEC is therefore in the weakly interacting regime for which the mean field description is relevant.